Hindawi
International Journal of Energy Research
Volume 2023, Article ID 8300877, 20 pages
https://doi.org/10.1155/2023/8300877

Research Article

Numerical and Optimization-Based Study on Split Hemispherical Shaped Fins for Augmenting Heat Transfer Rate

Alok Ranjan[1], **Ranjan Das**[2], **Sameer S. Gajghate**[3], **Debabrata Barik**[4], **Himadri Majumder**[3], **Elaine M. Cardoso**[5,6], **Arindam Majumder**[1], **Sagnik Pal**[1] and **Madhujit Deb**[1]

[1]*Mechanical Engineering Department, National Institute of Technology Agartala, 799046, Tripura, India*
[2]*Department of Mechanical Engineering, Indian Institute of Technology Ropar, 140001, Punjab, India*
[3]*Mechanical Engineering Department, G H Raisoni College of Engineering & Management, 412207, Pune, Maharashtra, India*
[4]*Department of Mechanical Engineering, Karpagam Academy of Higher Education, 641021, India*
[5]*Department of Mechanical Engineering, UNESP-São Paulo State University, UNESP Campus of Ilha Solteira, Av. Brasil 56, Ilha Solteira, SP 15385-000, Brazil*
[6]*Department of Mechanical Engineering, UNESP-São Paulo State University, Campus of São João da Boa Vista, São João Da Boa Vista, Brazil*

Correspondence should be addressed to Sameer S. Gajghate; mtech_sameer@yahoo.in
and Debabrata Barik; debabrata.barik@kahedu.edu.in

Received 9 November 2022; Revised 11 January 2023; Accepted 17 January 2023; Published 3 February 2023

Academic Editor: Sunday Olayinka Oyedepo

This paper deals with the numerical investigation of split hemispherical fins mounted staggered over a base plate. The thermal and flow analyses have been carried out to evaluate the Nusselt number (Nu), pressure drop (ΔP), and hydrothermal performance factor (HTPF) with air as a medium and Reynolds number (Re = /3000 to 15000). The cylindrical fin (CF) and hemispherical fin (HF, of radius R) of the same volume and height have been formed and placed in the computational domain. Results reveal that the Nu for CF compared to HF is 1.3-1.4 times higher, with approximately 1.5 times higher ΔP for the given Re range. The value of HTPF for HF is greater than unity (/1.13-1.20) for all the considered Re values. Secondly, the HF gets split into longitudinal and transverse flow directions for better solid-fluid interaction. The geometrical parameters are transverse offset TO (/=0 – R/8), longitudinal offset LO (/=0 – R/8), and Re. Results show that the highest value of Nu (/=384.10) and HTPF (/=1.33) have been obtained at TO = R/10 (at LO =0) and TO = R/10 (at LO = R/10) for the highest Re (/=15000). At last, the cuckoo search algorithm (CSA) coupled with the response surface method (RSM) has been performed to fetch the optimum value of Nu based upon dimensionless TO*, dimensionless LO*, and Re. The optimum value (obtained at TO* = 0.1, LO* = 0, and Re = 15000) of Nu (=/392.16) from CSA is promising, with the numerically obtained Nu value (=/384.1059) with an error of 2.05%.

1. Introduction

The current technological advancement-based devices need proper heat dissipation and management for providing higher efficiency and usability. Devices viz. heat exchanger, heat sink, exhaust gas recirculation system, lithium-ion battery setup, and/or refrigeration units need some attached arena in terms of extended surfaces to channel the excess heat to the surrounding. The use of fins, metal foams, phase change material, vortex generators, baffles, solid blocks, and roughness elements are promising. Here, consideration is given to conventional fins, as they are simple to design, economical, and easy to manufacture. Sabbaghi et al. [1] have done an analytic study to account for the thermal efficiency of semispherical fins under fully wet conditions and proposed a linear correlation between fin surface temperature

and humidity. Bi et al. [2] have done numerical analysis on dimple shape, low fin, and cylindrical groove fins using the field synergy principle. It has been seen that the PEC (performance evaluation criterion) value for dimple shape is higher than the cylindrical groove, followed by the low fin. The study also shows that a deep dimple with a larger diameter significantly affects augmenting heat transfer. Liu et al. [3] have done numerical work to understand the thermal and fluid flow physics of dimple-attached rectangular cooling channels along with hemispherical protrusion. Results show that the hemispherical protrusion helps provide downward flow, reattachment, and strengthen the vortex shedding. Further, heat transfer can be increased upon increasing hemispherical protrusion height with pressure drop penalties. Wang et al. [4] have done experimental work to determine the thermal performance of louver fin, semidimple-shaped fin, and plain fin. The result shows that semidimple fins perform better than louver fins for higher fin pitch and lower frontal velocity due to the increased swirled motion phenomenon. Chen et al. [5] have experimentally analyzed the heat transfer characteristics of elliptical fins and compared them with circular fins. It has been seen that flow resistance for the former is lesser than the latter fin with a higher heat transfer rate. Dasore et al. [6] have conducted a numerical study to analyze the rectangular and elliptical-shaped fins for an air-cooled internal combustion engine. The results show that elliptical fins have better heat augmentation capabilities than rectangular fins. Jin et al. [7] have numerically worked to see the effect of fin geometry on heat transfer using circular, elliptical, oblong, lancet, teardrop, and NACA profile-shaped fins. It has been noted that the NACA and teardrop-shaped fins are much better at transferring heat than the lancet, circular, elliptical, and oblong-shaped fins. Chimres et al. [8] have done a numerical study to analyze the fin tube-based heat exchanger with an elliptical winglet. A study reveals that an elliptical winglet with a fin tube shows higher thermal performance than a fin tube-based heat exchanger. Wang et al. [9] have done experimental and numerical investigations to see the thermal and fluid flow characteristics of circular, elliptical, and drop-shaped fins. The study reveals that the drop fins are better at suppressing the flow separation at the wake region and thus lead to less frictional loss than circular fins. Chyu et al. [10] have experimentally analyzed the effect of cubic, diamond, and circular fin geometry over heat transfer augmentation. It has been seen that cubic shaped fins yield higher heat transfer, followed by diamond and circular shaped fins with pressure drop penalties. Chang et al. [11] have experimentally studied twisted tape pin-fin arrays to enhance the heat transfer rate and thermal performance factor. Results reveal that the twisted tape arrays provide vertical induced flow, leading to an increase in the Nu number compared to the plain tube pin-fin array. Saravanakumar and Kumar [12] have done an experimental investigation for augmenting the heat transfer using pin-fin with surface texture in terms of a metric, worm, ACME, buttress, Sharpe V, and square thread. It has been seen that the textured pin fins provide a higher heat transfer rate with a lesser pressure drop penalty than the plain pin fin, and it also provides higher flow turbidity and delays the flow separation. Naphon and Sookkasem [13] have experimentally analyzed the thermal and flow behavior of taper-based pin-fin heat sinks. It has been seen that taper-based geometry helps reduce the pressure drop, and further, the work is validated with numerical work and found to be in good agreement. Sara et al. [14] have experimentally analyzed the effect of geometrical parameters on Nu and friction factor (f) on square cross-section pin-fin with second law analysis. Results reveal that the interfin distance and clearance ratio greatly affect Nu and f. Further, the smaller entropy generation is associated with a lower Re value with a higher value of interfin distance ratio and interfin spacing ratio. Peles et al. [15] have done an experimental and analytical study for micropin-fin under a forced convective environment. A concise discussion on thermal resistance, which is affected by geometrical and thermohydraulic parameters, has been done. Tahat et al. [16] have done experimental work to see the effect of an inline and staggered arrangement of pin-fin mounted over a base plate. Further, a correlation for Nu (based on Re, fin height, and fin pitch) has been developed individually for inline and staggered arrangement. Sahiti et al. [17] have numerically analyzed the thermal and fluid flow performance of NACA, drop form, lancet, elliptical, circular, and square-shaped fins. The elliptical pin-fin is better, whereas the NACA profile does not affect pressure drop much as the formers fins. Li and Wang [18] have studied the heat transfer and pressure drop characteristics of louver fins placed in a condenser test section. Based on the experimentation, a correlation has been established between heat transfer and pressure drop. Zhang et al. [19] have done an experimental and numerical investigation on W-type fins-based heat sink and compared it with the plate-fin heat sink. It has been noted that the W-type fin shows a higher cooling effect than the plate-fin heat sink. Gao et al. [20] have used a multijet impinging system with a trapezoidal fin array to increase the efficiency of the electronic device. It has been seen that both the unilateral and bilateral jet arrangements augment the thermal performance. Shaeri and Yaghoubi [21] have numerically analyzed the solid and perforated pin-fin for a given range. Results show that the longitudinal perforation enhances the solid and fluid interaction, reduces weight, and decreases the wake formation at the trailing edge of the fin. Jonsson and Moshfegh [22] have done analytical work to predict the Nu and pressure drop of the plate-fin array, an inline and staggering array of strip fins, circular fins, and square-shaped fins. It has been seen that using a pin-fin heat sink at a high Reynolds number for zero bypass duct is not beneficial. Raja et al. [23] have used a heat transfer search algorithm to optimize the various geometrical parameters associated with a fin tube-based heat exchanger. It has been noted that the optimized geometrical parameters minimize the weight and cost of the heat exchanger, and further, a comparative analysis is performed using a genetic algorithm, particle swarm optimization, and artificial bee colony algorithm. Jyothiprakash et al. [24] have used a genetic algorithm and particle search algorithm in order to get the optimum value of geometrical parameters to maximize (hot fluid effectiveness) and minimize (number of

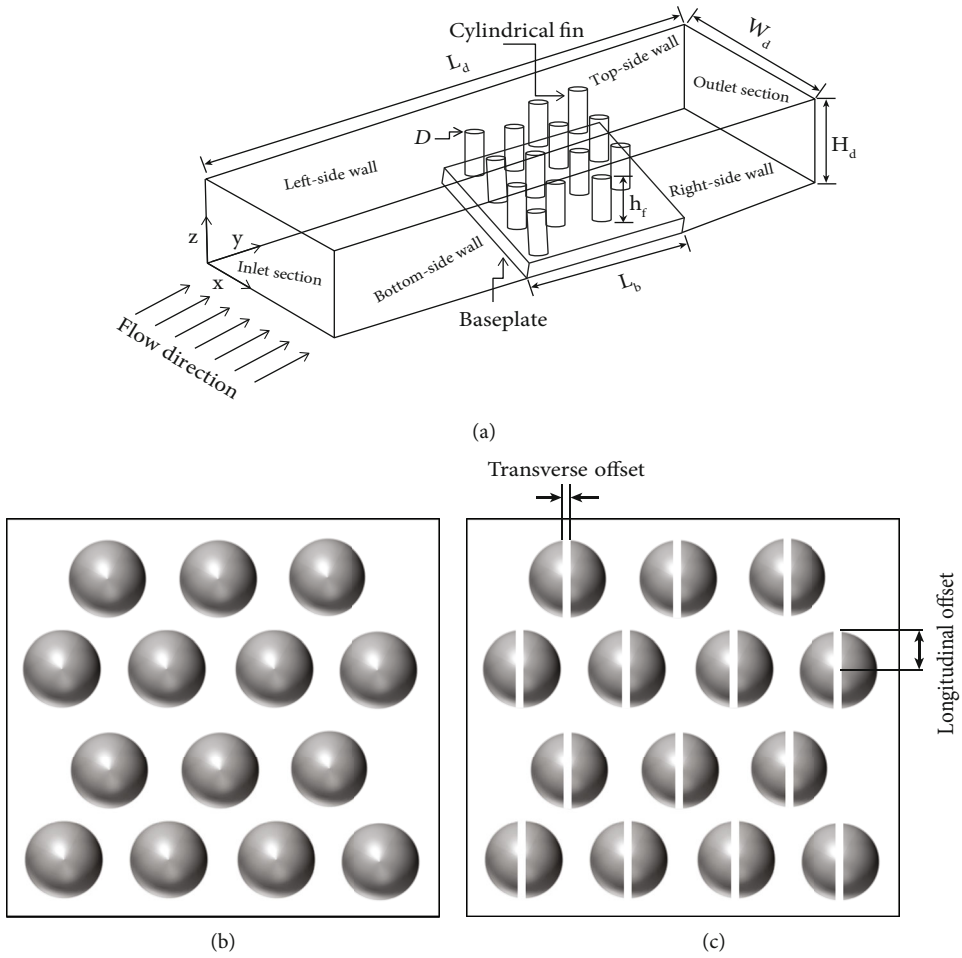

Figure 1: Schematic diagram of (a) cylindrical fins setup with computational domain, (b) hemispherical fin, and (c) split-based hemispherical fin.

entropy generation units) for three fluids cross-flow-based plate-fin heat exchanger. It has been seen that particle swarm optimization (PSO) needs lesser computational duration for convergence over GA for single-objective optimization. Ranjan et al. [25] have worked on numerical analysis of offset-based elliptical fins using the cuckoo search algorithm and obtained the optimum value of the Nusselt number. Das and Kundu [26] have used modified differential evolution (MDE) search algorithm to determine the optimum value of heat transfer rate, fin efficiency, and effectiveness for T-shaped wet fins. Das and Kundu [27] have determined the optimum value of fin thickness using a differential evolution search algorithm to obtain the maximum heat transfer rate value. They found that fin thickness's role is evident in getting a higher heat transfer rate.

Although the work based on convectional fins has been analyzed experimentally and numerically by several researchers, the work on split-based hemispherical fins in the longitudinal and transverse direction of fluid flow is not being analyzed yet. The novelty of the work lay behind the use of a hemispherical fin with different split widths in both the transverse and longitudinal direction, which helps in the intermixing of fluid at the trailing end. So, in that order, the performance parameters viz. Nusselt number, frictional factor, pressure drop, and hydrothermal performance factor (HTPF) have been numerically analyzed in the present work over the Re range (3000-15000) using ANSYS 19. At last, to fetch the maximum value of Nu based upon dimensionless offsets and Re, a correlation has been developed using the response surface method coupled with the cuckoo search algorithm.

2. Geometry and Formulations

The attached arena has always controlled thermal dissipation and its associated properties in terms of extended surface fins. Here, the work consideration is given to the cylindrical and hemispherical fins mounted over a base plate. Figure 1(a) shows a schematic diagram of 14 cylindrical fins of diameter D (/=17.96 mm) and height h_f (=/11 mm) mounted over a base plate of dimension $100 \times 100 \times 3\,\text{mm}^3$ placed in the computational domain. The length (L_d), width (W_d), and height (H_d) of the computational flow domain are 1040 mm, 100 mm, and 15 mm, with the inlet section and outlet section of the computational flow domain being 28.54 and 7.47 times the hydraulic mean diameter D_h (/=0.0261 mm), respectively. The schematic diagram of cylindrical fins, hemispherical fin, and split-

Table 1: Boundary condition for computational work.

Inlet-side	Velocity u with constant temperature $T_{\text{inlet}} = 300\,\text{K}$
Outlet-side	Pressure outlet $P_{\text{gauge}} = 0\,\text{Pa}$ with constant temperature $T_{\text{outlet}} = 300\,\text{K}$
Left-side, right-side, top-side, and bottom-side walls	No slip condition with adiabatic walls
Base plate	Constant heat flux $(Q_b) = 6000\,\text{W/m}^2$

based hemispherical fin are shown in Figure 1. The dimension of HF is obtained upon equating its volume to the CF (as shown in Figure 1(b)) volume. Further, the modification of fins has been done using split, i.e., longitudinal offset (LO) and transverse offset (TO) varying from 0 to $R/8$ (where R (/=11 mm) is the radius of HF), as shown in Figure 1(c).

The heat transfer phenomenon is mathematically represented for any system using the energy equation. The radiation mode of heat transfer is neglected in the present study and the convective and conductive mode of heat transfer is analyzed thoroughly. The thermal behavior of any flow domain is analyzed using thermal potential and is related to the temperature difference. Hence, to understand the temperature field in the flow domain, the energy equation needs to be solved. Upon neglecting the volumetric heat generation, the energy equation [28] is mentioned in Equation (1). Similarly, in the above equation, the term T requires an understanding of the velocity field $\vec{u}$. Hence, the velocity field accounted in the given flow domain (Figure 1(a)) requires the solution of mass and momentum conservation. Altogether, these mass and momentum conservation equations can be furnished using Equations (2) and (3). The boundary condition plays a vital role in order to assign the temperature as well as velocity field upon solving Equations (1) to (3). The assigned boundary condition are mentioned in Table 1 are numerically computed to the computational setup. Here, ANSYS fluent 19, a finite volume method-based solver, is used to predict the thermal and fluid flow behavior of a fin setup placed in a computational domain.

The coupled scheme is used for velocity and pressure coupling, and the Green-Gauss node-based spatial gradient discretization was considered.

$$\rho c_p \nabla \bullet \left(\vec{u} T\right) = \nabla \bullet (k \nabla T), \tag{1}$$

$$\nabla \bullet \left(\rho \vec{u}\right) = 0, \tag{2}$$

$$\rho \vec{u} \bullet \nabla \vec{u} = \mu \nabla^2 - \nabla P. \tag{3}$$

The prime focus of the current work is to evaluate the thermal and fluid flow characteristics of fin setup mounted over a base plate placed in a computational fluid flow domain. Hence, the Nusselt number Nu is evaluated to gauge the relative rate of convective heat transfer to the conductive heat transfer, mentioned in Equation (4). In order to assign the velocity boundary condition, the value of Re (based on the inlet section of the computational domain) is evaluated using Equation (5). Similarly, to account the frictional losses into the flow domain, the frictional factor based upon inlet and outlet pressure is depicted in Equation (6). Now, upon gauging the pressure drop, it is very important to counter the usability of particular fins w.r.t. the base fin (CF). For that, the hydrothermal performance factor (HTPF) is evaluated using Equation (7). Now, the flow condition lies in the turbulent regime; hence, the turbulent-based k-ϵ model is used. The terms turbulent kinetic energy (k) and turbulent kinetic energy dissipation (ϵ) are mentioned using Equations (8) and (9), whereas the associated constant terms used are obtained using comprehensive curve fitting over the turbulent flow range [29, 30].

$$\text{Nu} = \frac{Q_b \bullet D_h}{k_f \left(T_f - ((T_o - T_i)/2)\right)}, \tag{4}$$

$$\text{Re} = \frac{u \bullet D_h}{\vartheta} \text{ where } D_h = \frac{4A_c}{P_C}, \tag{5}$$

$$f = \frac{(\Delta P / L_c) D_h}{(1/2)\rho_f u^2}, \tag{6}$$

$$\text{HTPF} = \frac{Nu/Nu_o}{\Delta P/\Delta P_o} \text{ where } \Delta P = P_{\text{inlet}} - P_{\text{outlet}}, \tag{7}$$

$$\text{div}\left(\rho k \vec{u}\right) = \text{div}\left[\left(\frac{\mu_t}{\sigma_k} \text{ grad } k\right)\right] + 2\mu_t E_{ij} \bullet E_{ij} - \rho\varepsilon, \tag{8}$$

$$\begin{aligned}\text{div}\left(\rho \varepsilon \vec{u}\right) == d\text{iv}\left[\left(\frac{\mu_t}{\sigma_\varepsilon} \text{ grad } \varepsilon\right)\right] + C_{1\varepsilon}\frac{\varepsilon}{k} 2\mu_t E_{ij} \\ \bullet E_{ij} - C_{2\varepsilon}\rho\frac{\varepsilon^2}{k}.\end{aligned} \tag{9}$$

3. Grid Independence Test and Validation

Any numerical investigation needs a grid independency test to procure the accurate velocity and temperature field for discretizing governing Equations (1)–(3). The current numerical work has focused on CF and HF (of the same volume and height) mounted over a base plate in a computational domain. In order to fetch better results from CFD (computational fluid dynamics), a better quality mesh is always recommended. Thus, tetrahedron meshing approach is used for analyzing the variation of parameters in the present study. Further, a grid dependency test has been carried out individually to know the average surface fin temperature and skin friction factor fluctuation over the number of finite volume method (FVM) grids. It has been found that fluctuations between 2.8×10^6 and 3.5×10^6 number of FVM grids are approximately lesser than 0.02% (both fins setup) and 0.11% (<0.055% for hemispherical fins setup), as shown in Figure 2. Hence, further analysis has been carried out using the FVM grid lying in between 2.8×10^6 and 3.5×10^6.

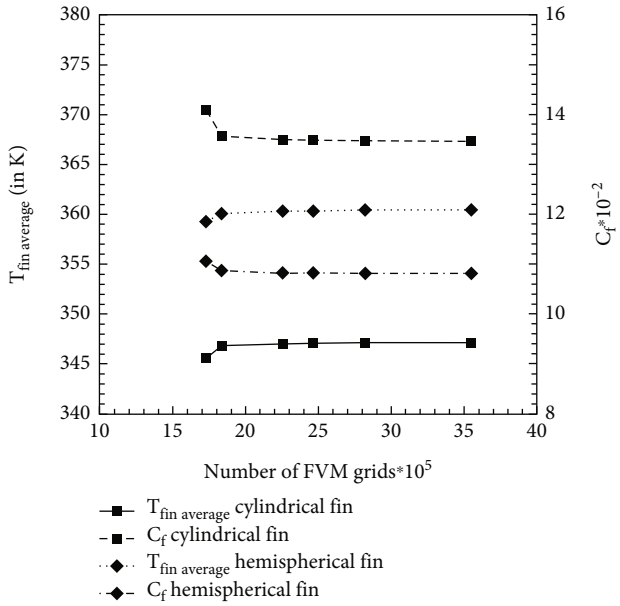

Figure 2: Grid test for cylindrical and hemispherical fin geometry.

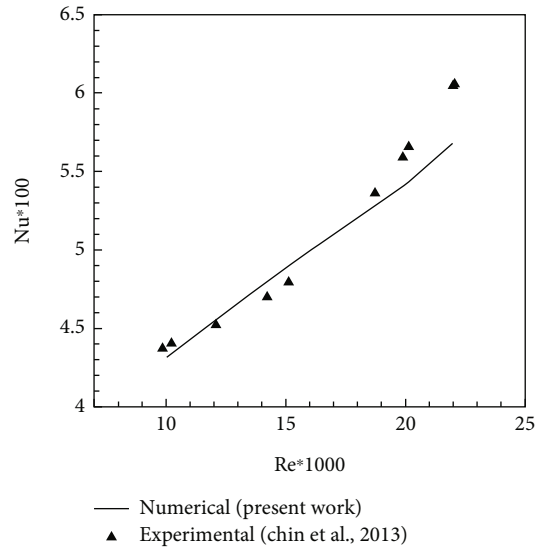

Figure 3: Validation plot of Nu vs. Re range.

For validating the solver, the present numerical solutions have been compared with the experimental work of [28]. For that, a rectangular cross-section-based computational domain has been considered with 14 circular fins with diameter D (/=8 mm) and height h_f (/=50 mm) mounted over a heated base plate of area A_b ($100 \times 110\,mm^2$) and thickness t_b (3 mm). The inlet section of the computational domain has been assigned with inlet temperature ($T_{inlet} = 300\,K$) with airflow velocity (Re = 10000, 15000, 20000, and 22000). The outlet section has been set with outlet gauge pressure ($P_{gauge} = 0\,Pa$) and outlet temperature ($T_{outlet} = 300\,K$), and the base plate has provided a constant heat flux condition ($Q_b = 6000\,W/m^2$). Upon validation, the minimum and maximum Nu variation compared to experimental work was 0.67% and 8.2% at Re = 10000 and 22000, as shown in Figure 3.

4. Methodology for Mathematical Model and Optimization

4.1. Response Surface Method. The response surface method (RSM) is a widely used, basic mathematical, and experimental tool for establishing the desired objective function. The RSM is mainly used when several variables are affecting the response function. It mainly works for first- and second-order polynomial functions. The first-order model is useful when the response is defined using the linear function of the variable; otherwise, second-order model is established. Here, in the present work, the variables, i.e., dimensionless terms, may affect the response parameter in an ascent or decent manner; hence, the second-order model is established. The following are detailed steps followed in the present study:

(i) Firstly, collect the data from the numerical simulation in terms of input variables (dimensionless parameters, i.e., TO*, LO*, and Re) and the desired output (Nusselt number). Further, the response function and independent variable data are used to make the response surface plot

(ii) Establish the second-order model using the input variables (consisting of 1st-order model and both the quadratic and cross-product term) and further use the full factorial method of design of experiment to get the approximate response function in terms of Nusselt number (Nu), i.e., fitting the second-order model

(iii) Thirdly, make the ANOVA table (for analysis of the variables' effect on response function) and analyze the various design of the experiment model. Further examine the P value and coefficient of determination, i.e., R^2, which leads to providing the information of correct prediction of the response variable (Nu) upon using the given independent variable (i.e., dimensionless terms)

However, the mathematical response function (Nu) in accordance with the independent variables has developed using RSM, and it is mentioned in Results and Discussion.

4.2. Cuckoo Search Optimisation. Here, the cuckoo search optimization has been used to carry out the obtained single-objective function based on the response surface method. Cuckoo search optimization has a diverse capability to solve various optimizations based on engineering problems. It uses the switching parameter to maintain stability amid local and global variables while operating the global optimization. The cuckoo is a bird whose egg laying strategy has attracted global scientific researchers, i.e., the cuckoo never makes its own nest and lays its eggs in the other bird's nest. The cuckoo carries away the host bird nest to provide a good possibility of hatching. Furthermore, if the host bird

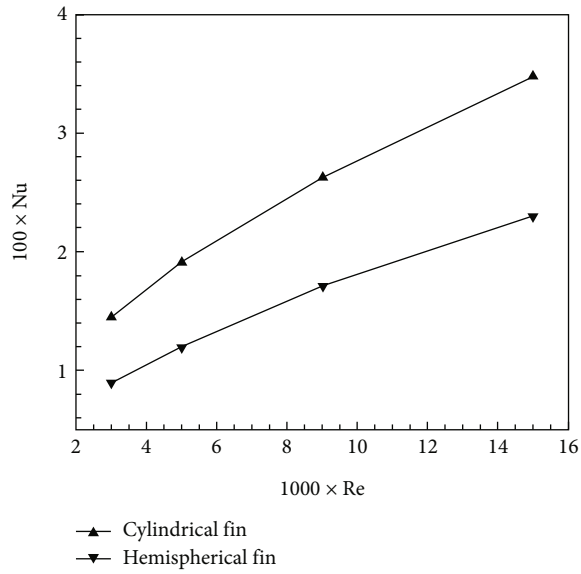

Figure 4: Comparison of cylindrical and hemispherical fins for Nusselt number (Nu) varying with different Re values.

finds the eggs of some other bird, she either destroys the cuckoo egg or finds a new home. And this unique behavior of the cuckoo bird led to the formation of the cuckoo search algorithm with three basic steps mentioned as follows:

(1) Each cuckoo bird simultaneously drops one egg in a randomly selected nest

(2) The finest egg badge in a nest will be considered the prime nest and imparted to the new generation

(3) At last, the host bird's nest is properly defined, and the probability of different eggs recognized by the host bird is Pa {0,1}. Further, upon finding the cuckoo egg, the host bird may shatter the egg or fly away to construct a new nest

With the help of Levy flight (as shown in Equation (10)), the cuckoo's new offspring can be established in the cuckoo search algorithm.

$$x_j(i+1) = x_j(i) + \beta n^{-\lambda}, \tag{10}$$

where $\beta > 0$, $1 \le \lambda \le 3$.

5. Results and Discussions

Determining the various parameters associated with the accounting performance of the extended surfaces needs proper analysis. The Nusselt number (Nu), which is used for determining the relative gain in the rate of convective to conductive heat transfer should be investigated, and further, the pressure drop (using inlet and outlet section) should be analyzed for obtaining the frictional losses in the system. Moreover, for determining the usability of the fin as compared to the base fin, the hydrothermal performance factor (HTPF) needs to be determined. The value of HTPF is obtained using the performance parameter viz. Nu and pressure drop, i.e., the relative gain in the heat transfer rate to the relative gain in the pressure drop.

Initially, the value of the Nu number has been accounted for the CF and HF for all the considered ranges of Re. The Nu values for CF (=/161.88, 213.72, 297.46, and 393.44) are 1.3-1.4 times higher than the HF (=/118.59, 155.56, 223.61, and 303.68) for all considered Re (=/3000, 5000, 9000, and 15000) ranges, as shown in Figure 4. It is mainly due to the shape form, i.e., the cylindrical shape has early flow separation, which in turn provides more recirculation zone at the wake region of fins and thus leads to provide more duration of solid-fluid interaction, whereas due to the shape, the fluid glides over the HF, delaying the flow separation and reducing the duration of solid-fluid interaction, leading to a reduced convective to conduction heat transfer rate. The temperature plot for cylindrical fin and hemispherical fin for different Re is shown in Figure 5. It can also be concluded from Figures 5(a)–5(d) that the surrounding fluid average temperature in the last row and the subsequent fin rows are greater (which indirectly implicates the lesser fin surface temperature) for the cylindrical fin compared to the hemispherical fin at the given Re number. Thus, the CF shows higher heat dissipation, i.e., a higher Nu value than the laHF for all the given Re ranges. The Nu value increases with Re for both CF and HF, as shown in Figure 4. Further, as the Re increases from 3000 to 15000, the turbulence level in the conduit increases, and return provides better fluid intermixing, which in turn alleviates rate of heat transfer, as shown in Figure 6. It can be seen from Figures 6(a)–6(d), i.e., the CF have more flow separation which in turn creates more frictional losses and thus alleviates the rate of heat transfer than the HF.

Figure 7 portrays the comparison of cylindrical and hemispherical fins for pressure drop and friction factor, varying with different Re values. The pressure drop increases with an increase in Re for both the CF and HF. However, the ΔP value is approximately 1.5-1.6 times lower for HF (=/26.76, 64.08, 183.64, and 459.93) than CF (=/41.4, 100.15, 285.61, and 715.68) at corresponding Re (=/3000, 5000, 9000, and 15000) ranges, as shown in Figure 7(a). Further, the frictional loss in the system has also been accounted for using the frictional factor, and it has been found to recede upon increasing Re value, as shown in Figure 7(b). It may be because, upon increasing Re, the turbulence level is elevated and suppresses the boundary layer growth. However, the frictional loss is pronounced more for the CF setup than HF one due to the flow separation delay associated with hemispherical fins.

Further, the value of HTPF has been accounted for HF upon treating the CF as the base case. The value of HTPF for H is greater than unity (=/1.1334, 1.1375, 1.1691, and 1.2011) for all the considered Re (=/3000, 5000, 9000, and 15000) ranges, as mentioned in Figure 8. It is mainly because the lower pressure drop accounted for HF compared to the CF one. The higher value of HTPF for hemispherical fins provides a chance of modification in terms of the split, which has been done in the further sections.

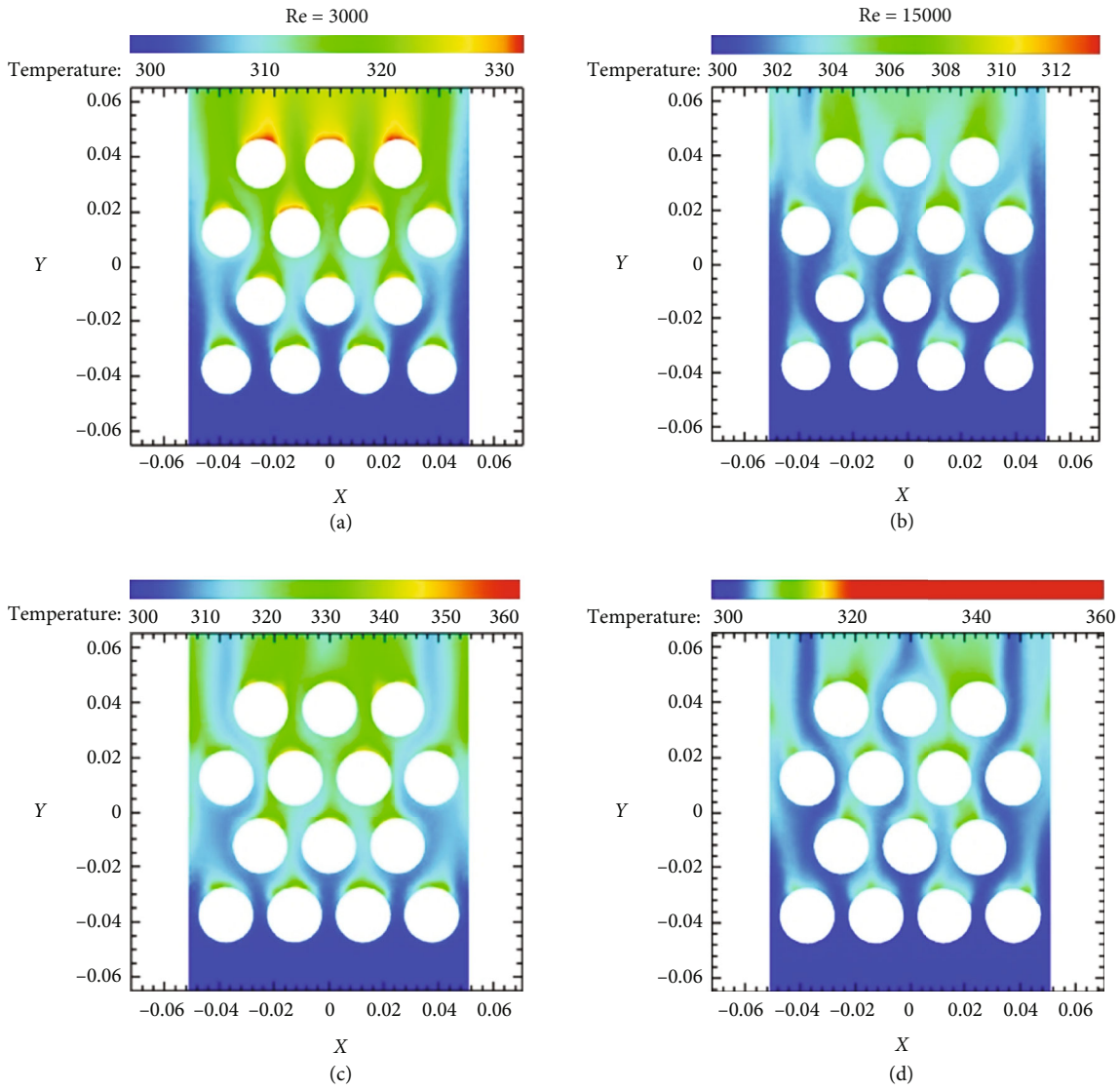

FIGURE 5: Temperature plot for (a, b) cylindrical fin and (c, d) hemispherical fin for different Re drawn at z plane (0.0075 m above the base plate).

6. Effect of Transverse Split

Upon analyzing the HF, work has been forayed toward doing splits in the transverse direction of fluid flow. The value of Nu has been accounted for TO = R/10, R/9, and R/8 over the considered range of Re. At Re = 3000, the values of Nu for TO = R/10, R/9, and R/8 (=/154.23, 153.28, and 149.17) are 23.10%, 22.63%, and 19.33% times higher than the solid hemispherical fin (=/118.59). Similarly, the Nu value has been accounted for in all considered values of Re, and it has been found that the highest value of Nu (/=384.10) is accounted for TO = R/10 at Re = 15000, as shown in Figure 9. Sahel et al. [31] have also worked over the hemispherical shape of the fin with further modification in terms of holes through it (case 1-6) and found the highest Nu value for case 6 (which is 2.08% lesser than the highest value of the current work), as shown in Figure 9. The superior value of Nu as compared to the given reference has motivated for analyzing the other parameters with further modification in terms of a split in both the transverse and longitudinal direction. The highest Nu is pronounced for lesser split width (TO = R/10) because the ease of flow in between the gap increases as its width increases from R/10 to R/8. Further, it can also be seen from Figure 10 that the higher fluid temperature is encompassed by a lesser width gap, i.e., R/10, which indirectly shows lesser fin temperature and thus augments a higher rate of heat in terms of Nu.

Similarly, the effect of friction factor f, which depends upon the pressure drop, has accounted for all the values of Re for a transverse split-based hemispherical fin. At Re = 3000, the value of f for TO = R/10, R/9, and R/8 (=/0.4049, 0.4010, and 0.3986) are 16.15%, 15.82%, and 14.97% times higher than the solid hemispherical fin (=/0.3389). Similarly, corresponding to other values of Re (5000, 9000, and 15000), the value of f has been accounted and it has been seen that the f value decreases over increasing Re. As the Re increases, the intermixing increases and suppresses the flow separation, and this leads to reduce the rate of decrease of f for

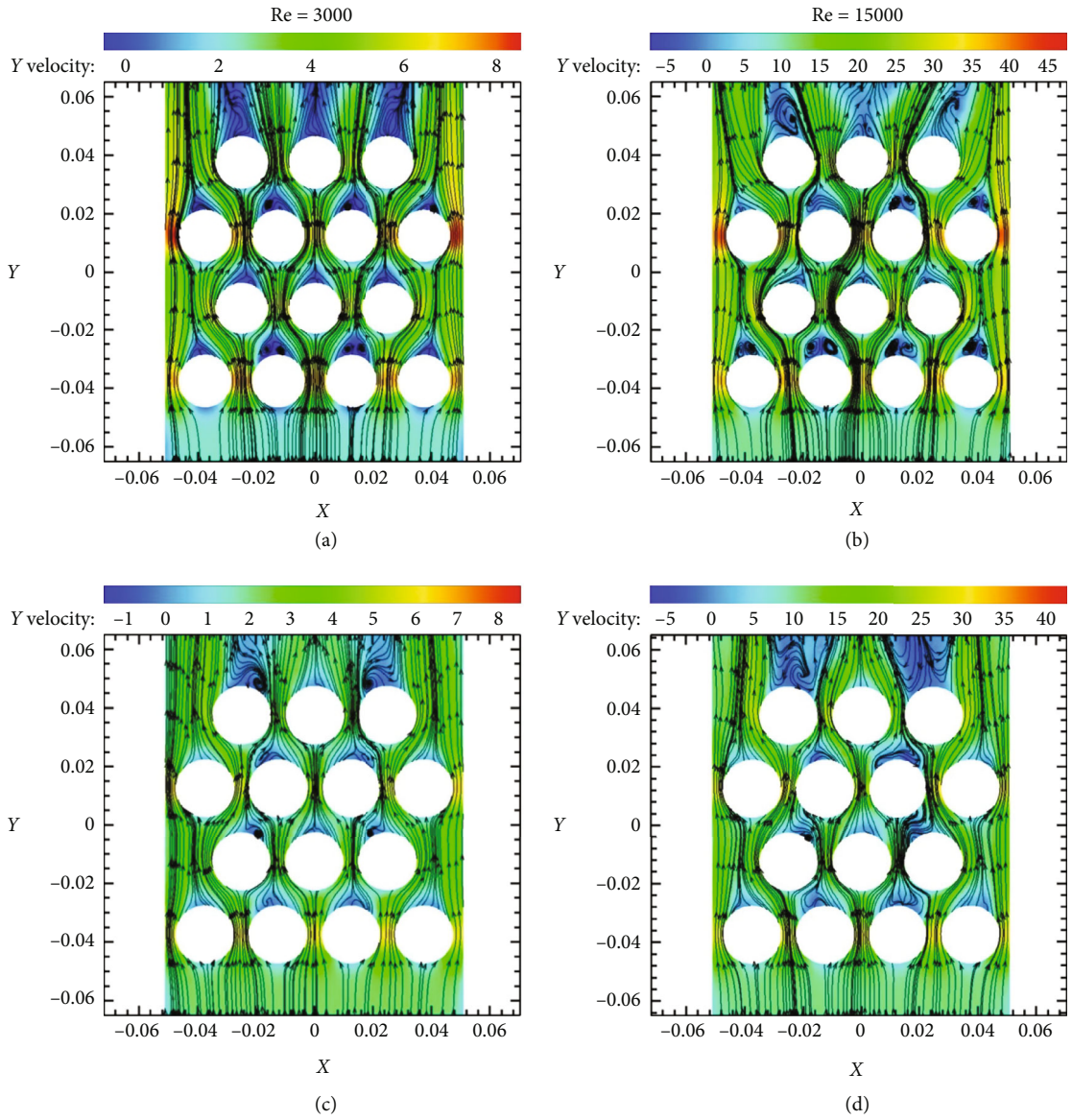

Figure 6: Streamline plot for (a, b) cylindrical fin and (c, d,) hemispherical fin for different Re drawn at z plane (0.0075 m above the base plate).

higher Re's. And thus, the highest value of f is found for TO = $R/10$ at Re = 3000, as shown in Figure 11. It can be seen from Figure 12 that a higher recirculation phenomenon is attached to the lower value of TO's as the ease of flow reduces, which in turn provides more frictional losses and that leads to augmenting the heat transfer. And, as the width gap increases, the frictional losses also decrease (i.e., the recirculation zone started diminishing) because flow can easily pass in between the gap and this leads to reduce the heat transfer rate.

Further, the value of HTPF has accounted for all the values of Re for unsplitted and TO-based split HF (upon considering CF set up as a base case at respective Re). It can be seen from Figure 13 that, the value of HTPF increases as the Re increases for both the unsplitted and splitted HF. It is mainly because, as the Re increases the value of Nu increases (due to an increase in turbulence level), and the friction loss decreases (which is mainly due to a delay in flow separation over an increase in Re). The value of HTPF for TO = $R/10$, $R/9$, and $R/8$ are 1.2753, 1.2703, and 1.2592 at Re = 15000, and similarly, the value of HTPF are accounted for other Re's at respective TO's, as shown in Figure 13. Upon splitting the fins the pressure drop reduces leading to receding the frictional loss in the system and thus augments the heat transfer. Further, upon increasing TO from $R/10$ to $R/8$, the ease of fluid flow increases with a reduction in pressure drop (the extent of recirculation recedes), resulting in the reduction of HTPF value.

7. Effect of Combined Offset Split

The analysis of performance parameters has been done upon varying TO from $R/10$ to $R/8$. Further, at fixed TO, the value of LO will vary from 0 to $R/8$ for all the considered Re (3000

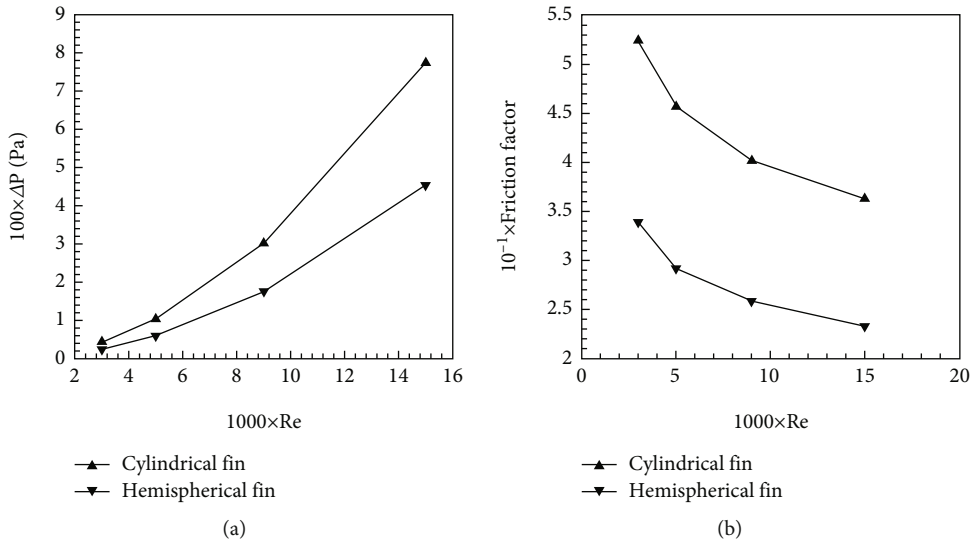

Figure 7: Comparison of cylindrical and hemispherical fins for (a) pressure drop (ΔP in Pa) and (b) friction factor varying with different Re values.

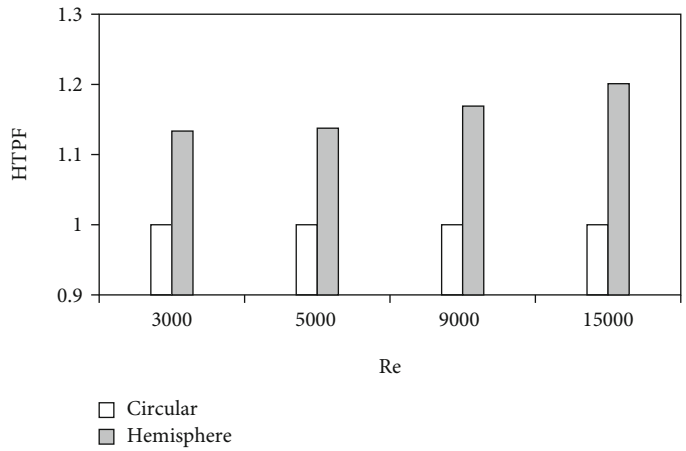

Figure 8: Comparison of HTPF value of hemisphere with cylindrical fin (base case) at different Re values.

to 150000). It has been found that, upon varying LO from 0 to $R/9$, the value of the Nu number decreases, and further from $R/9$ to $R/8$, it increases for the fixed value of TO = $R/10$ and $R/9$, as mentioned in Figure 14. The decrement of Nu for LO varying from 0 to $R/9$ (at TO = $R/10$ and $R/9$) is based on the fact that as the LO increases from 0 to $R/9$, the fluid can easily pass in between the gap and also from either side. And, this will reduce the frictional losses which in turn recedes the Nu value. Further, upon varying the LO from $R/9$ to $R/8$, the flow may pass easily in between the gap but a flow resistance would be offered from either side as the interfin gap reduces to more extent. The above remarks regarding the variation of Nu w.r.t to the given split gap, i.e., TO and LO, can also be understood using Figure 15. (as part of supplemental material). It shows that at a fixed value of TO = $R/10$ and $R/9$, the fluid temperature is lesser for LO (varying from 0 to $R/9$) and vice versa for LO (varying from $R/9$ to $R/8$), which directly affects the average fin temperature, and thus initially Nu decreases (from LO = 0 to $R/9$) and increases (from LO = $R/9$ to $R/8$).

Now, varying LO from 0 to $R/9$ at TO = $R/8$, the value of Nu gets increases and further gets decreases as LO changes from $R/9$ to $R/8$, as mentioned in Figure 14. The extent of the recirculation phenomenon is much more pronounced (because the interfin gap at TO = $R/8$ is very less, which in turn provides flow resistance, and this flow resistance gets reduces as LO varies from 0 to $R/9$ and again increases as LO changes from $R/9$ to $R/8$). And this variation in the extent of circulation phenomenon affects the average fluid and the fin temperature, i.e., surrounding fluid temperature increases for LO (0 to $R/9$) and decreases for LO (changing from $R/9$ to $R/9$), as shown in Figure 15 (as part of supplemental material).

Further, upon varying LO (0 to $R/8$) at a fixed value of TO's, the value of frictional losses has been evaluated for all the considered Re ranges, as shown in Figure 16. It has

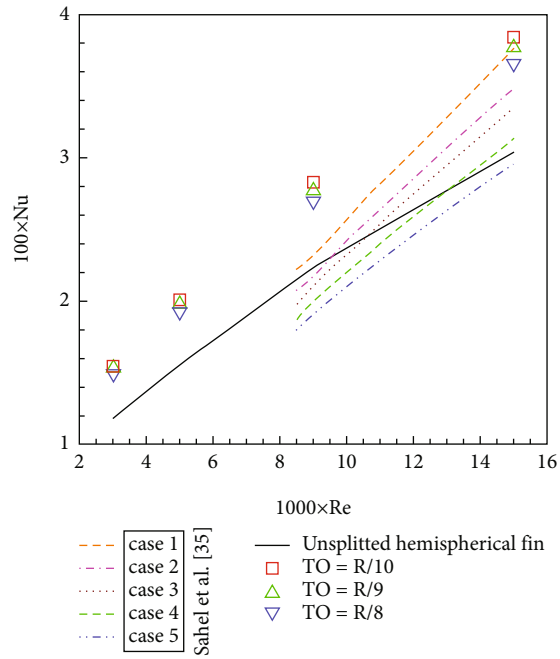

FIGURE 9: Variation of Nu vs. Re for unsplitted and TO-based split-based hemispherical fin with comparison with Sahel et al. [31].

been found that the friction factor (based upon the pressure drop) gets reduced upon increasing LO from 0 to $R/9$ and further gets increases from LO = $R/9$ to $R/8$ (at fixed TO = $R/10$ and $R/9$). It may be because lesser flow resistance is offered due to the ease of fluid flow in between the fins to the incoming fluid upon changing LO from 0 to $R/9$, which leads to a lesser extent of recirculation phenomenon at the fin wake and vice versa for LO changing from $R/9$ to $R/8$, as mentioned in Figure 17 (as part of supplemental material). However, upon varying LO from 0 to $R/9$ (at fixed TO = $R/8$), the frictional losses increase and further decrease as LO changes from $R/9$ to $R/8$. It may be because, upon changing LO from 0 to $R/9$ (at fixed TO = $R/8$), flow can pass in between as well as from either side, i.e., it contributes from both ways, whereas the higher flow resistance comes into phenomenon from either side of the fins, when LO changes from $R/9$ to $R/8$, leading to reduce the heat transfer rate.

Moreover, the HTPF value provides the fins usability upon gauging the relative gain in Nu w.r.t relative gain in pressure drop. The highest value of HTPF (/=1.33) is accounted for TO = LO = $R/10$ at Re = 15000, as shown in Figure 18. The illustration of the involved step for fetching out optimum Nu using CSA is shown in Figure 19. The highest obtained value of HTPF is mainly because the fin (at TO = LO = $R/10$) is vigorously contributing to enhancing the heat transfer rate from either side as well as in between the fin gap. The relative gain in pressure drop is much lesser than the relative gain in Nu for all the considered split and unsplit HF and this leads to providing a higher (greater than unity) HTPF value than the CF. And, this remarks that splitting HF (in transverse as well as in longitudinal direction) requires less pumping effort than CF. Moreover, work done by Hempijid and Kittichaikarn [32] on the pin-fin-based heat sink, Tikadar et al. [33] on min-channel, and Alfellag et al. [34] over plate fin with inclined slotter over the range of Re found the HTPF value as 1.013, 1.42, and 1.54.

8. Mathematical Model Using RSM

For obtaining the mathematical model, the response surface method has utilized full factorial method of design of experiment with response parameter Nu and variable elements as dimensionless longitudinal offset LO*, dimensionless transverse offset TO*, and Re. The response surface method uses regression and a statistical approach to formulate the objective function, and the detailed step is mentioned in the reference [35]. In order to develop the approximate model, the response surface plot has been used as shown in Figures 20 and 21. Here, the numerical result forms the second-order polynomial function for Nu is obtained using MINITAB 17. The mathematical correlations have been formed with a determination coefficient R^2 of 99.90%, as given in Equations (11) and (12).

$$\begin{aligned}\mathrm{Nu} = {} & 92.37 + (0.026999 \times \mathrm{Re}) - (108.2 \times \mathrm{TO}^*) \\ & - (68.7 \times \mathrm{LO}^*) - (0.00000035 \times \mathrm{Re} \times \mathrm{Re}) \\ & + (337 \times \mathrm{LO}^* \times \mathrm{LO}^*) - (0.01266 \times \mathrm{Re} \times \mathrm{TO}^*) \\ & + (0.00006 \times \mathrm{Re} \times \mathrm{LO}^*) + (225 \times \mathrm{TO}^* \times \mathrm{LO}^*),\end{aligned} \tag{11}$$

for $3000 \le \mathrm{Re} \le 15000$, $\mathrm{TO}^* < 0.125$, and $0 \le \mathrm{LO}^* \le 0.125$.

The ANOVA for the Nu model for Equation (11) is given in Table 2.

$$\begin{aligned}\mathrm{Nu} = {} & 78.96 + (0.024491 \times \mathrm{Re}) - (72.6 \times \mathrm{LO}^*) \\ & - (0.00000035 \times \mathrm{Re} \times \mathrm{Re}) + (593 \times \mathrm{LO}^* \times \mathrm{LO}^*) \\ & + (0.00324 \times \mathrm{Re} \times \mathrm{LO}^*),\end{aligned} \tag{12}$$

for $3000 \le \mathrm{Re} \le 15000$, $\mathrm{TO}^* = 0.125$, and $0 \le \mathrm{LO}^* \le 0.125$.

Detail equations supporting the calculation of various parametric values are given in Table S1 (refer to supplementary material section).

The ANOVA for the Nu model for Equation (12) is given in Table 3.

9. Ratification of Mathematical Model

The two different mathematical correlations have been developed using input variables corresponding to the given constraint. Then, the accuracy of the developed model was checked using the P value mentioned in the ANOVA (Table 2) part of the supplemental material (for Equation (11)) and (Table 3) part of the supplemental material (for Equation (12)). Results show that the obtained value of P is less than 0.05 for both the developed model (mentioned as Equations (11) and (12)), which indirectly signifies better accuracy. Moreover, the determination coefficient (R^2) for adjusted R^2 has been examined to recheck the accuracy. As a result, the value for R^2 and adjusted R^2 for Equation (11)

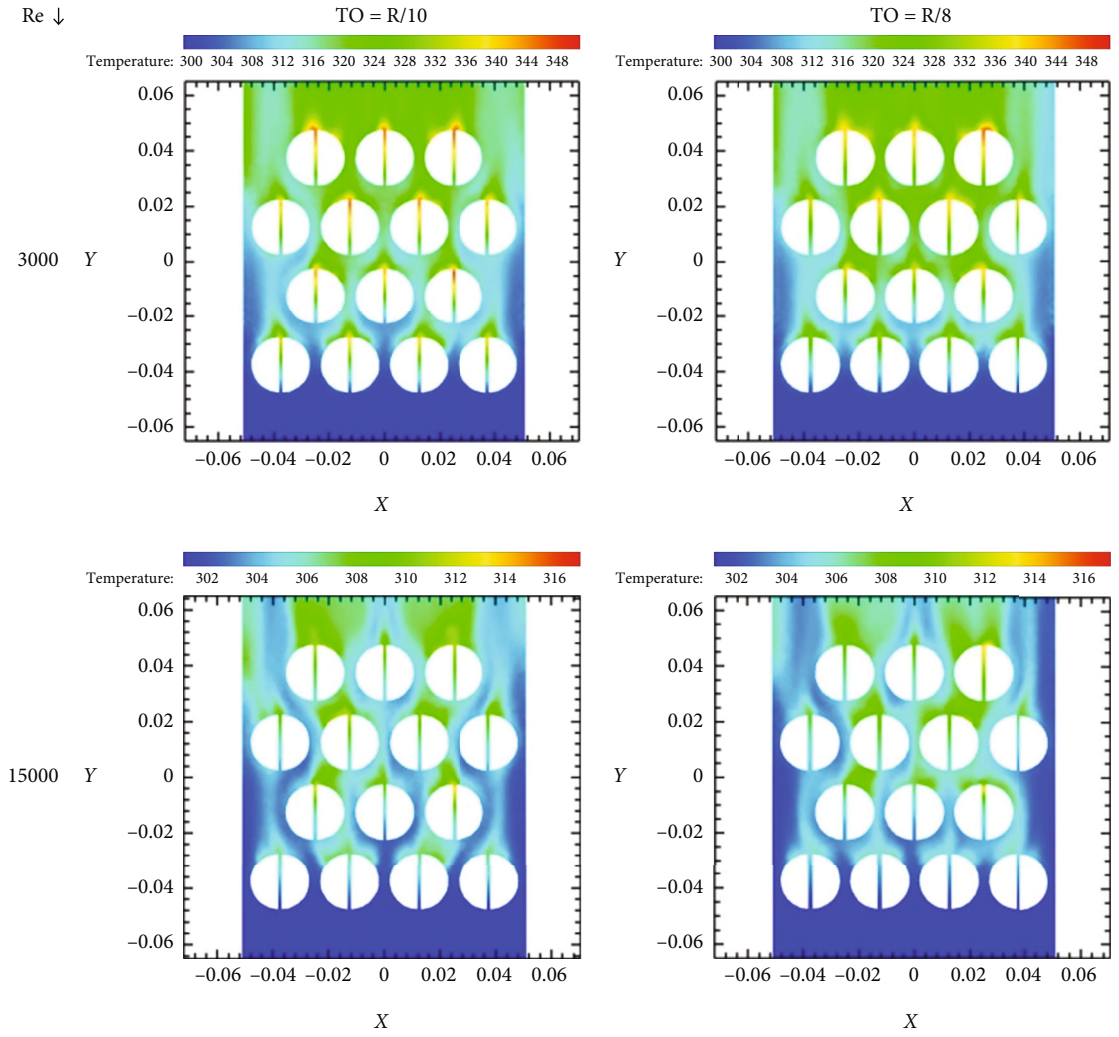

Figure 10: Temperature plots for TO-based split hemispherical fin at different Re values.

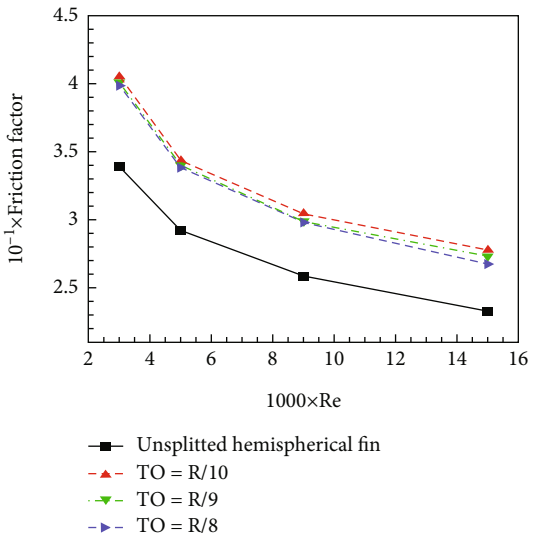

Figure 11: Variation of friction factor with different Re value for unsplitted and TO-based split-based hemispherical fin.

is 99.97% and 99.93% and for Equation (12), is 99.98% and 99.94%, respectively, which signifies higher accuracy (as both are greater than 90%).

10. CSA Outcomes

The cuckoo search algorithm (CSA) has been carried out for the offset-based hemispherical fin. The maximum value of the Nu number has been obtained at the optimum value of the said variable using CSA based upon a single-objective function. The CSA algorithm is embedded into MATLAB and executed using a workstation-based Intel Xeon CPU E31245 with 8 GB RAM (3.30 GHz).

For getting the optimum value of TO*, LO*, and Re, the desired step for CSA are mentioned in Figure 19, and also, the required steps are mentioned below:

(i) Commence the procedure by taking $M = 20$ (population size) and $n_{max} = 30$ (maximum iteration) with $Pa = 0.25$ (as probability factor) and $\lambda = 2$ (CSA parameter)

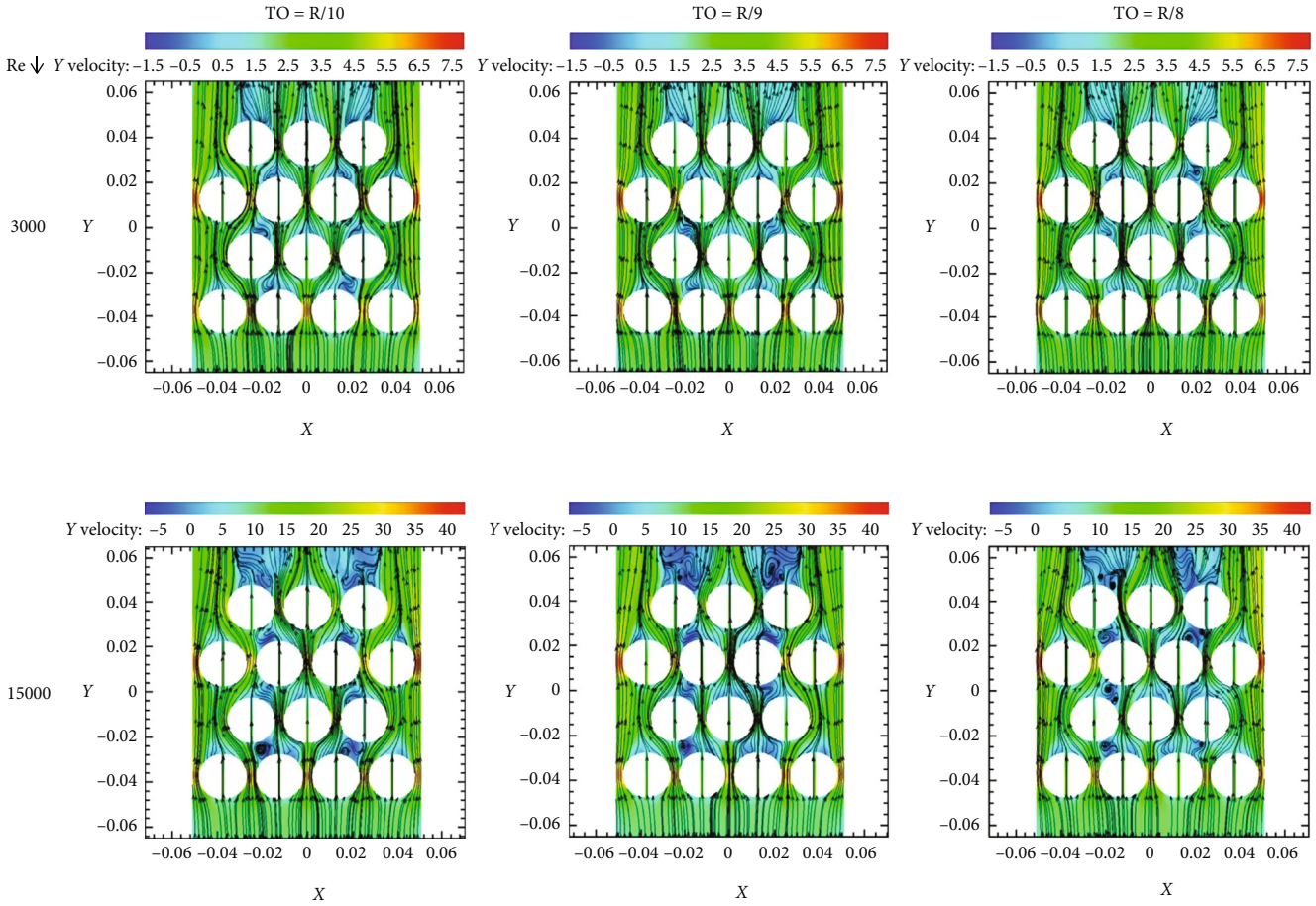

Figure 12: Streamline plots for TO-based split hemispherical fin at different Re values.

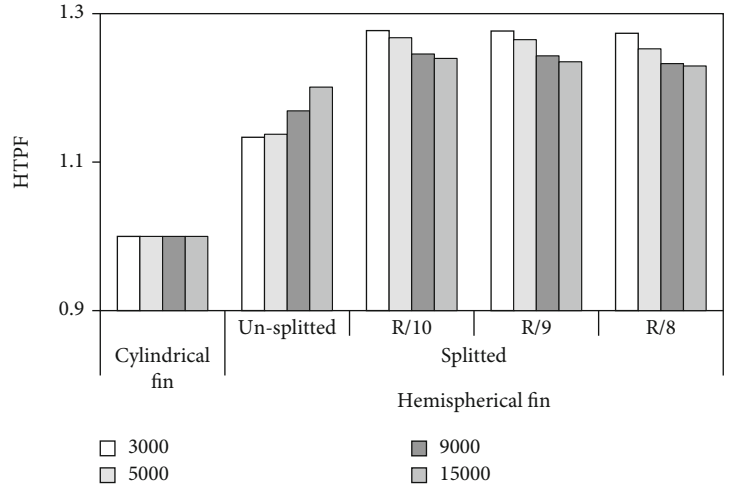

Figure 13: Variation of HTPF for various fins geometry at different Re number values.

(ii) Arbitrarily create and site the M number of host bird nests. The obtained former nest should be well characterized by arbitrarily selected. The arbitrarily created nest location is well described by the randomly opted Re, TO*, and LO* (as input within the given range of extent)

(iii) Start by taking the first iteration n equals zero

(iv) Further, take $n = n + 1$ as the subsequent iterations

(v) Exhibit the Nu (as a fitness value using Equations (11) and (12)) for the opted host nest

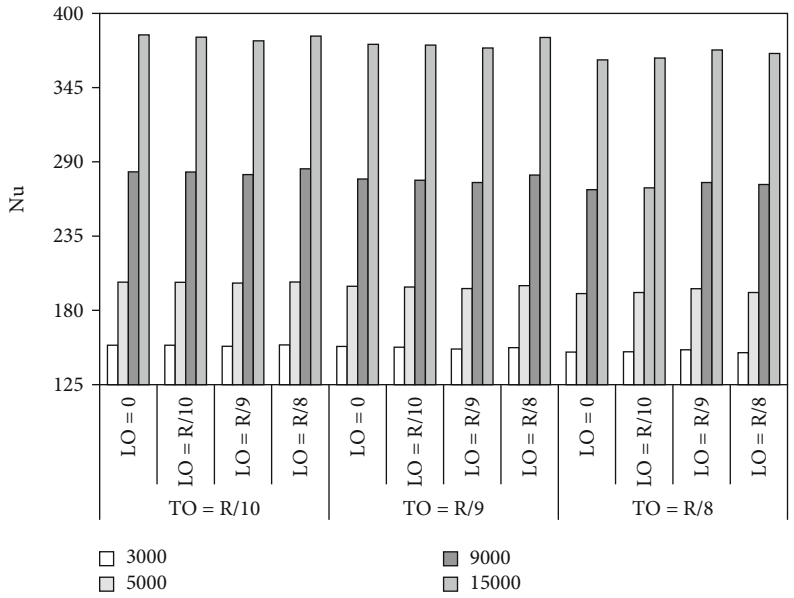

Figure 14: Variation of Nu for varying LO's at fixed value of TO's over the range of Re.

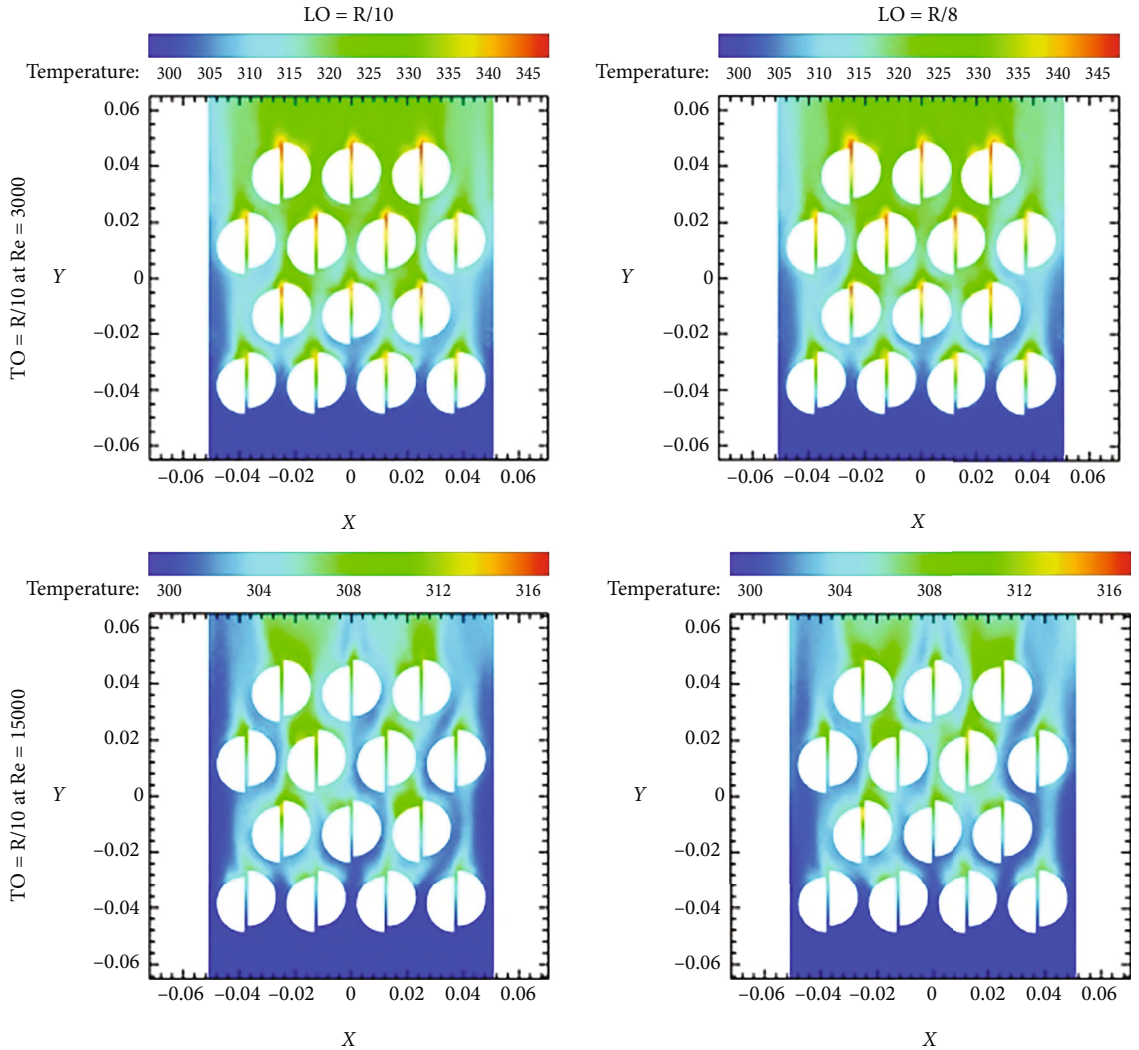

Figure 15: Temperature plot z plane (0.075 m from origin) for varying LO's at fixed TO's at different Re numbers.

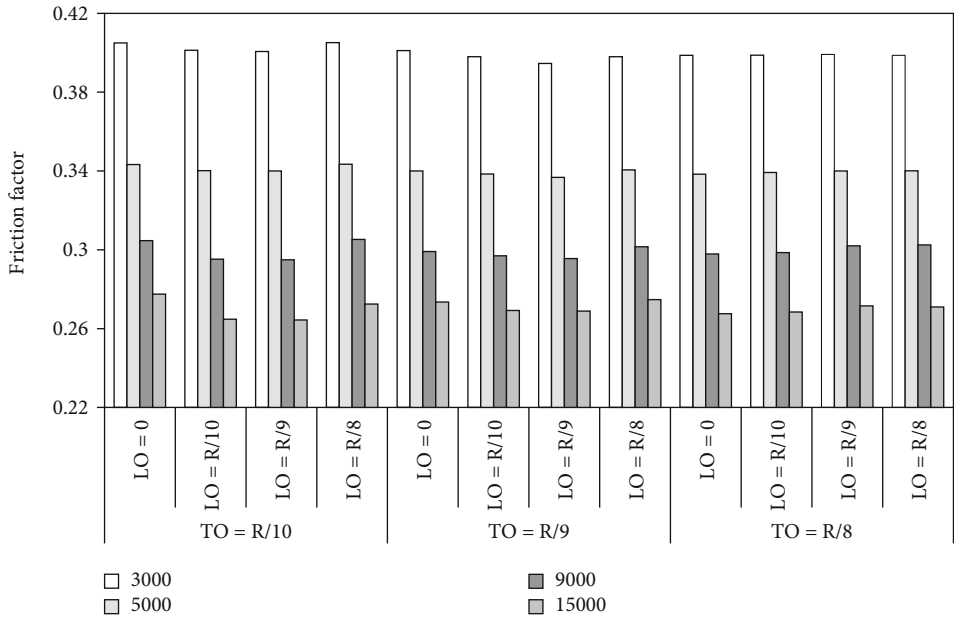

Figure 16: Variation of friction factor with different values of Re for varying LO's at fixed TO's.

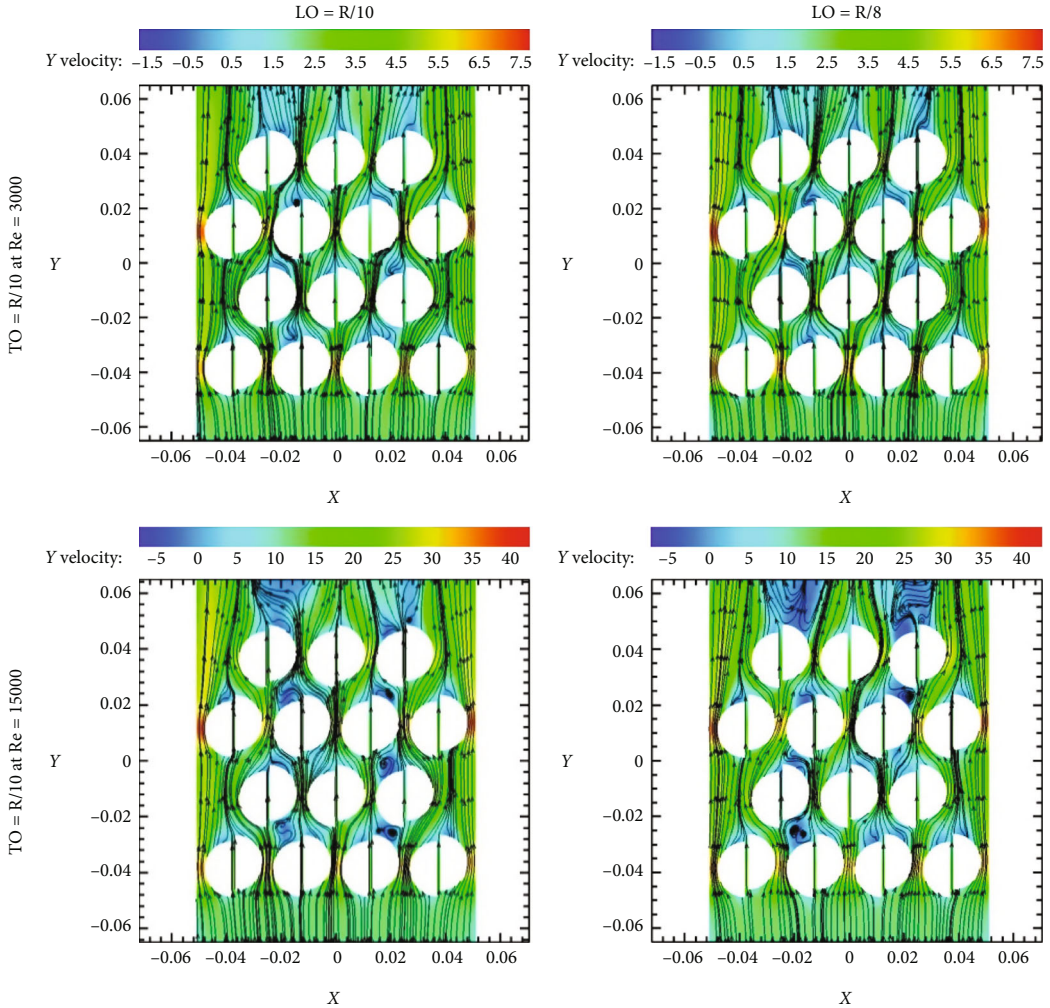

Figure 17: Velocity plot z plane (0.075 m from origin) for varying LO's at fixed TO's at different Re numbers.

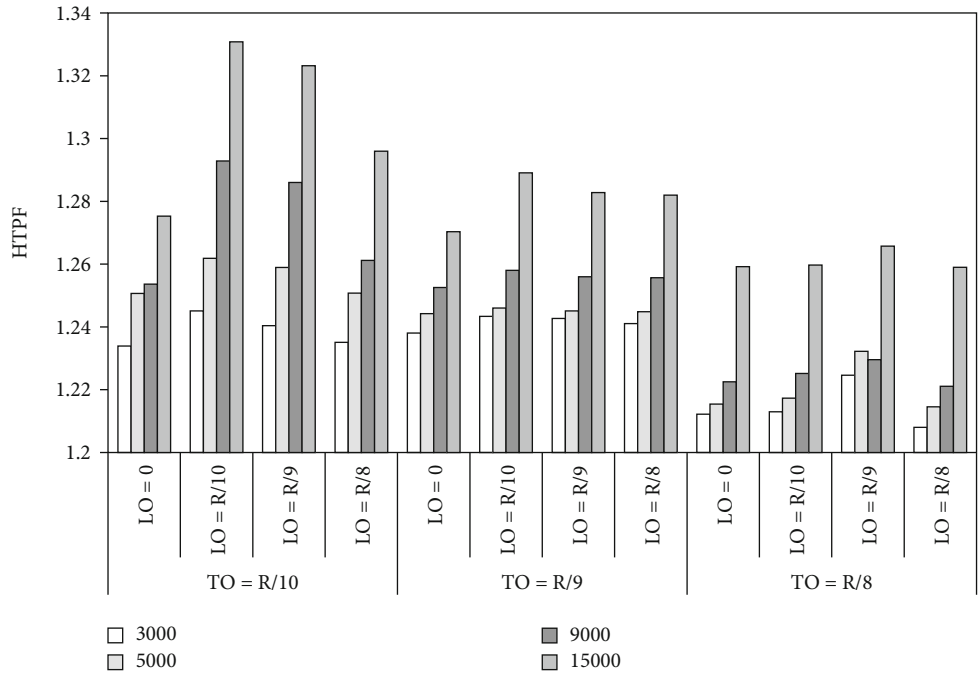

Figure 18: Variation of HTPF for varying LO's at fixed TO's over the Re range.

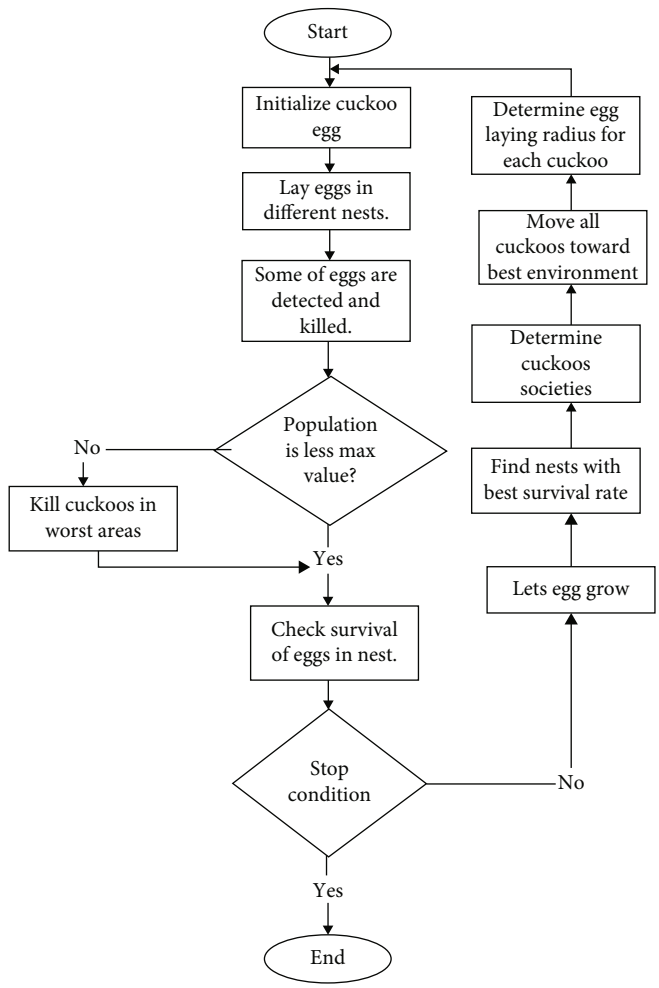

Figure 19: Illustration of the involved step for fetching out optimum Nu using CSA.

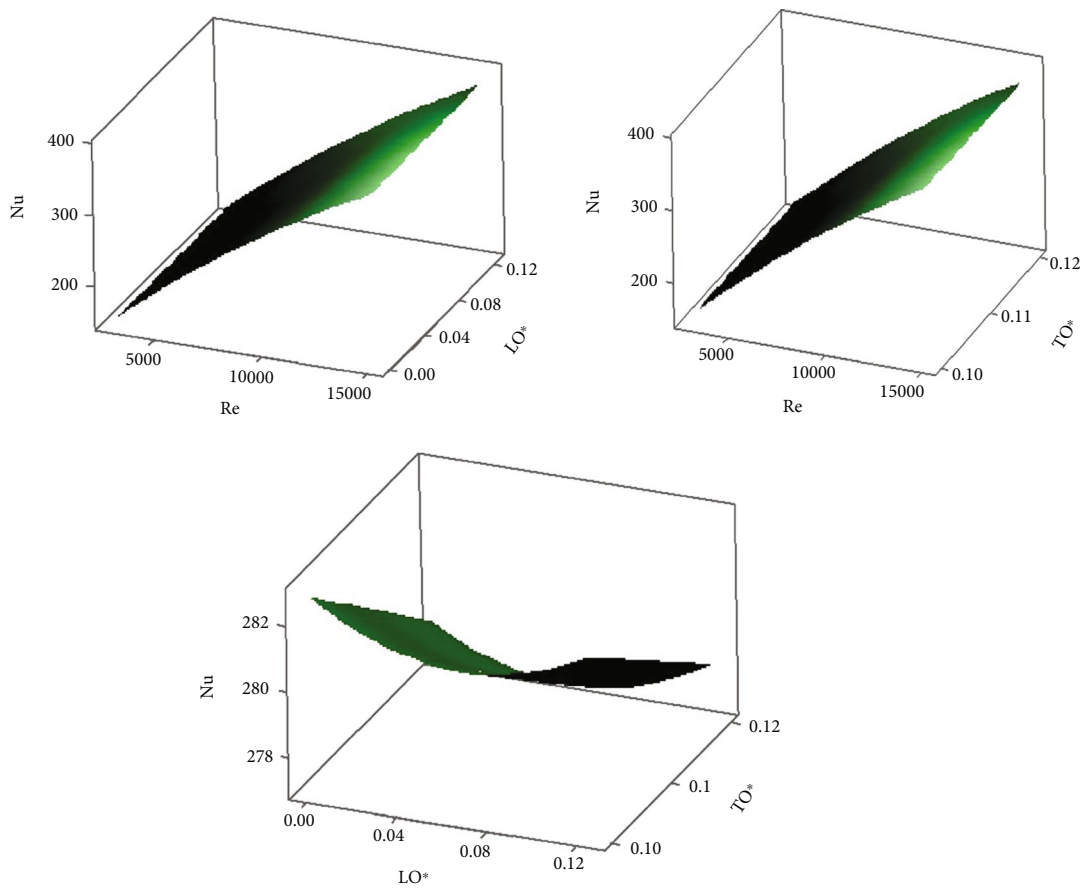

Figure 20: Response surface plot of Nu w.r.t input parameters if $3000 \leq \mathrm{Re} \leq 15000$, $\mathrm{TO}^* < 0.125$, and $0 \leq LO^* \leq 0.125$.

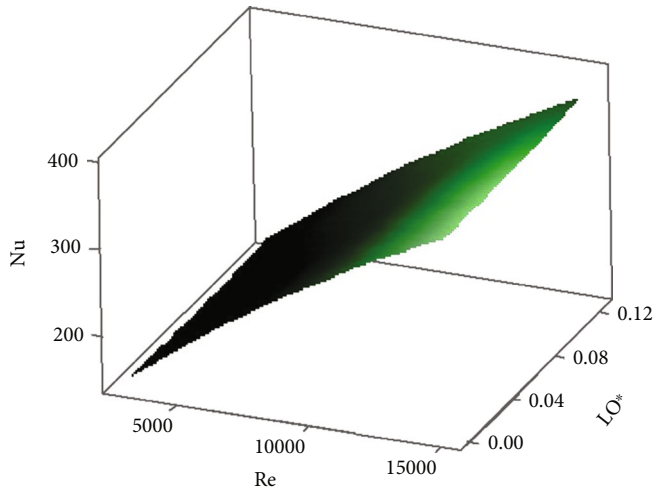

Figure 21: Response surface plot of Nu w.r.t input parameters $3000 \leq \mathrm{Re} \leq 15000$, $\mathrm{TO}^* = 0.125$, and $0 \leq \mathrm{LO}^* \leq 0.125$.

(vi) Investigate the entire opted nest and look out for such nest which is providing maximum value of Nu and takes that as the best nest out of all

(vii) In order to get the new nest further, use Equation (10)

(viii) Again find out the Nu for $x_i(n+1)$

(ix) Randomly spot and take a nest $x_j(n)$ from the given M (population size) and eventually study and equate with $x_i(n+1)$

(x) Examine the former result, i.e., whether $x_i(n+1)$ comes out to be better than $x_j(n)$ and if so, then former $(x_i(n+1))$ by later $(x_j(n))$

Table 2: ANOVA for the Nu model for Equation (11).

Source	DF	Adj SS	Adj MS	F value	P value
Model	8	237613	29702	8603.27	$P \le 0.001$
Linear	3	196422	65474	18964.94	$P \le 0.001$
Square	2	1020	510	147.80	$P \le 0.001$
2-way interaction	3	11	4	1.08	0.377
S	1.85806		R^2	99.97%	
R-sq(adj)	99.95%		R^2 (pred)	99.93%	

Table 3: ANOVA for the Nu model for Equation (12).

Source	DF	Adj SS	Adj MS	F value	P value
Model	5	111363	22272.5	9752.54	$P \le 0.001$
Linear	2	91621	45810.6	20059.21	$P \le 0.001$
Square	2	478	239.1	104.69	$P \le 0.001$
2-way interaction	3	9	9.1	3.97	0.074
S	1.51121		R-sq	99.98%	
R-sq(adj)	99.97%		R-sq(pred)	99.94%	

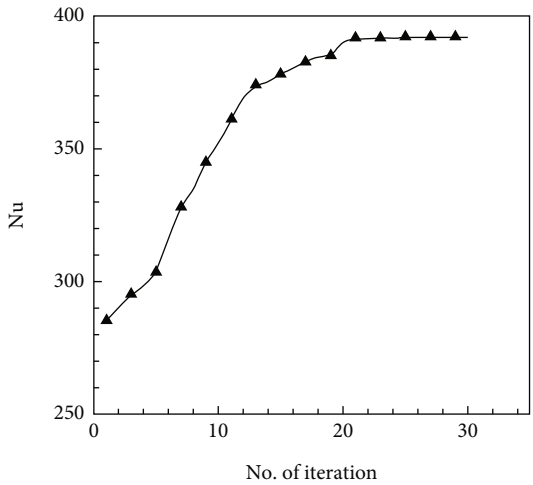

Figure 22: Convergence plot for Nu vs. number of iterations obtained using CSA.

(xi) Now, upon studying the considered nest, sort out them as per the receding order of Nu vale

(xii) Out of the taken nests, replace the probability factor (Pa) of the nest pertaining least Nu value (which is obtained using Equation (10)).

(xiii) Lastly, repeat step number 4, if the number of iterations is lesser than n_{max} else, move to the upcoming step

(xiv) Lastly, obtain the best solution with its correlated Nu

Table 4: Validation of the developed model with optimal parameter settings.

Parameters	Re	TO*	LO*	Nu
Predicted	15000	0.1	0	392.16
Experimented	15000	0.1	0	384.1059
Error percentage (%)				2.05

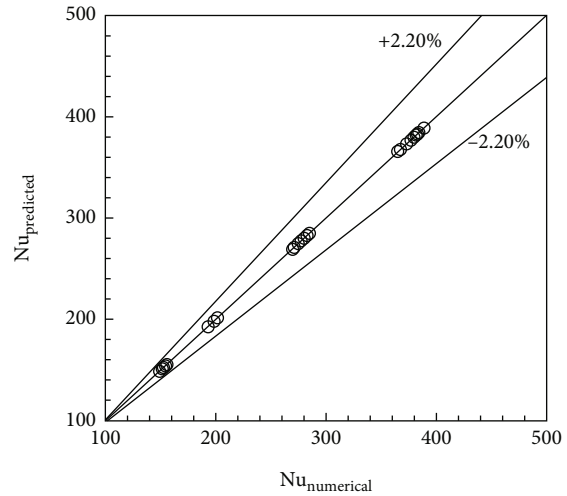

Figure 23: Comparative analysis of Nu based upon CSA and numerical.

The convergence trait of the cuckoo search algorithm obtained while solving the said problem is mentioned in Figure 22. Further, the desired objective, i.e., to fetch the maximum value of the Nusselt number corresponding to the independent variables TO*, LO*, and Re using CSA, is obtained with 2.05% accuracy compared to numerical work, depicted in Table 4. At last, a comparison plot has been presented between the CSA and numerically obtained outcomes, which are within ±2.20%, as depicted in Figure 23.

11. Conclusions

The prime focus of the current work is to augment the heat transfer phenomenon using an HF. Initially, the CF was validated using established experimental work and found to be in order with reasonable accuracy. Further, the longitudinal and transverse offsets-based split modification is done to elevate the heat transfer with pressure drop penalties. The split-based fins help augment the heat transfer upon creating a recirculation zone at the fins' wake. For the small split gap, the difficulty of fluid flow between the gap leads to a higher frictional loss in the system, leading to more solid-fluid interaction. A previous work [25] has numerically worked on split elliptical-based fins and found the highest value of PEC (performance evaluation criterion) as 1.225, whereas the highest value of HTPF in the present work is 1.33. The other vital points based on the current work are mentioned below:

(i) The value of HTPF for the HF is higher than the CF. It is due to lower pressure drop penalties associated with a lower Nu value than the cylindrical fin

(ii) The hemispherical shape helps the fluid glide over it, thus delaying the flow separation. In contrast, the early flow detachment in CF augments Nu at higher pressure drop penalties

(iii) Upon splitting the HF, the Nu value increases with a slight frictional loss

(iv) Upon increasing TO, the ease of fluid flow increases and reduces the frictional loss; thus, the heat transfer rate also reduces

(v) Upon increasing LO at fixed TO, the interfin gap changes, modifying the flow by creating the recirculation zone at the fins wake and affecting the heat transfer rate

(vi) The highest value of Nu (/=384.10) and HTPF (/=1.33) are obtained at TO = $R/10$ (at LO = 0 and $R/10$) for Re = 15000

(vii) The response surface method is used to develop a correlation for Nu based on independent variables (TO*, LO*, and Re)

(viii) The optimum value of Nu (/=392.16) is obtained at TO* = 0.1, LO* = 0, and Re = 15000 using CSA with an error of 2.20% compared to numerical work

Nomenclature

A_b: Base plate area (mm^2)
A_c: Channel cross-section area (mm^2)
CSA: Cuckoo search algorithm
c_p: Specific heat (J/(kg K))
D: Cylindrical fin diameter (mm)
D_h: Hydraulic mean diameter (mm)
f: Frictional factor
h_f: Fin height (mm)
H_d: Computational domain height (mm)
HTPF: Hydrothermal performance factor
k_f: Fluid thermal conductivity (W/(m K))
L_b: Base plate length (mm)
L_d: Length of computational domain (mm)
LO: Longitudinal offset (mm)
LO*: Longitudinal offset (dimensionless)
Nu: Nusselt number
Nu_o: Nusselt number of the base case
ΔP: Pressure drop (Pa)
ΔP_o: Pressure drop of base case (Pa)
Pa: Probability factor utilized in CSA
Pr: Prandtl number
Q_b: Heat flux (W/m^2)
R: Radius of hemispherical fin
Re: Reynolds number
n: Number of iterations
t_b: Base plate thickness (mm)
n_{max}: Maximum number of iteration
T_{outlet}: Outlet temperature (K)
T_f: Average fin surface temperature (K)
TO: Transverse offset (mm)
TO*: Transverse offset (dimensionless)
u: Inlet flow velocity (m/s)
$\vec{u}$: Velocity vector
W_d: Computational domain width (mm)
x: Host bird nest in CSA
X, Y, Z: Computational domain coordinates (m)
DF: Degree of freedom
F value: MS/MSE (mean square error)
SS: Square of sum
MS: Mean square
Adj: Adjusted
Pred: Predicted

Greek Symbols

β: Step size used in CSA
λ: Cuckoo search algorithm parameter
μ: Dynamic viscosity (Pa s)
ρ: Density (kg/m^3)

Data Availability

The data is available in the manuscript.

Conflicts of Interest

The authors declare that they have no conflict of interest.

Acknowledgments

The authors thank the Department of Chemical Engineering, National Institute of Technology Agartala, India, and Karpagam Academy of Higher Education (Deemed to be University), Coimbatore, India, for providing research facilities to carry out the research work.

Supplementary Materials

The equations used for calculating various parameters are given in Table S1 (Supplementary file). *(Supplementary Materials)*

References

[1] S. Sabbaghi, A. Rezaii, G. R. Shahri, and M. S. Baktash, "Analyse mathematique de l'efficacite d'une ailette semi-spherique avec transfert de chaleur et de masse simultanes," *International Journal of Refrigeration*, vol. 34, no. 8, pp. 1877–1882, 2011.

[2] C. Bi, G. H. Tang, and W. Q. Tao, "Heat transfer enhancement in mini-channel heat sinks with dimples and cylindrical grooves," *Applied Thermal Engineering*, vol. 55, no. 1-2, pp. 121–132, 2013.

[3] J. Liu, Y. Song, G. Xie, and B. Sunden, "Numerical modeling flow and heat transfer in dimpled cooling channels with

secondary hemispherical protrusions," *Energy*, vol. 79, pp. 1–19, 2015.

[4] C. C. Wang, K. Y. Chen, J. S. Liaw, and C. Y. Tseng, "An experimental study of the air-side performance of fin-and-tube heat exchangers having plain, louver, and semi-dimple vortex generator configuration," *International Journal of Heat and Mass Transfer*, vol. 80, pp. 281–287, 2015.

[5] Q. Li, Z. Chen, U. Flechtner, and H. J. Warnecke, "Heat transfer and pressure drop characteristics in rectangular channels with elliptic pin fins," *International Journal of Heat and Fluid Flow*, vol. 19, no. 3, pp. 245–250, 1998.

[6] A. Dasore, U. Rajak, R. Konijeti et al., "Comparative numerical investigation of rectangular and elliptical fins for air cooled IC engines," *Materials Today: Proceedings*, vol. 49, pp. 481–485, 2022.

[7] W. Jin, J. Wu, N. Jia, J. Lei, W. Ji, and G. Xie, "Effect of shape and distribution of pin-fins on the flow and heat transfer characteristics in the rectangular cooling channel," *International Journal of Thermal Sciences*, vol. 161, article 106758, 2021.

[8] N. Chimres, C.-C. Wang, and S. Wongwises, "Effect of elliptical winglet on the air-side performance of fin-and-tube heat exchanger," *International Journal of Heat and Mass Transfer*, vol. 123, pp. 583–599, 2018.

[9] F. Wang, J. Zhang, and S. Wang, "Investigation on flow and heat transfer characteristics in rectangular channel with drop-shaped pin fins," *Propulsion and Power Research*, vol. 1, no. 1, pp. 64–70, 2012.

[10] M. K. Chyu, Y. C. Hsing, and V. Natarajan, "Convective heat transfer of cubic fin arrays in a narrow channel," *Journal of Turbomachinery*, vol. 120, no. 2, pp. 362–367, 1998.

[11] S. W. Chang, P. S. Wu, W. L. Cai, and C. H. Yu, "Experimental heat transfer and flow simulations of rectangular channel with twisted-tape pin-fin array," *International Journal of Heat and Mass Transfer*, vol. 166, article 120809, 2021.

[12] T. Saravanakumar and S. D. Kumar, "Heat transfer study on different surface textured pin fin heat sink," *International Communications in Heat and Mass Transfer*, vol. 119, article 104902, 2020.

[13] P. Naphon and A. Sookkasem, "Investigation on heat transfer characteristics of tapered cylinder pin fin heat sinks," *Energy Conversion and Management*, vol. 48, no. 10, pp. 2671–2679, 2007.

[14] O. N. Şara, S. Yapıcı, M. Yılmaz, and T. Pekdemir, "Second law analysis of rectangular channels with square pin-fins," *International Communications in Heat and Mass Transfer*, vol. 28, no. 5, pp. 617–630, 2001.

[15] Y. Peles, A. Koşar, C. Mishra, C. J. Kuo, and B. Schneider, "Forced convective heat transfer across a pin fin micro heat sink," *International Journal of Heat and Mass Transfer*, vol. 48, no. 17, pp. 3615–3627, 2005.

[16] M. Tahat, Z. Kodah, B. Jarrah, and S. Probert, "Heat transfers from pin-fin arrays experiencing forced convection," *Applied Energy*, vol. 67, no. 4, pp. 419–442, 2000.

[17] N. Sahiti, A. Lemouedda, D. Stojkovic, F. Durst, and E. Franz, "Performance comparison of pin fin in-duct flow arrays with various pin cross- sections," *Applied Thermal Engineering*, vol. 26, no. 11-12, pp. 1176–1192, 2006.

[18] W. Li and X. Wang, "Heat transfer and pressure drop correlations for compact heat exchangers with multi-region louver fins," *International Journal of Heat and Mass Transfer*, vol. 53, no. 15-16, pp. 2955–2962, 2010.

[19] K. Zhang, M. J. Li, F. L. Wang, and Y. L. He, "Experimental and numerical investigation of natural convection heat transfer of W-type fin arrays," *International Journal of Heat and Mass Transfer*, vol. 152, article 119315, 2020.

[20] W. Gao, J. F. Zhang, Z. G. Qu, and W. Q. Tao, "Numerical investigations of heat transfer in hybrid microchannel heat sink with multi-jet impinging and trapezoidal fins," *International Journal of Thermal Sciences*, vol. 164, article 106902, 2021.

[21] M. R. Shaeri and M. Yaghoubi, "Numerical analysis of turbulent convection heat transfer from an array of perforated fins," *International Journal of Heat and Fluid Flow*, vol. 30, no. 2, pp. 218–228, 2009.

[22] H. Jonsson and B. Moshfegh, "Modeling of the thermal and hydraulic performance of plate fin, strip fin, and pin fin heat sinks-influence of flow bypass," *IEEE Transactions on Components and Packaging Technologies*, vol. 24, no. 2, pp. 142–149, 2001.

[23] B. D. Raja, V. Patel, and R. L. Jhala, "Thermal design and optimization of fin-and-tube heat exchanger using heat transfer search algorithm," *Thermal Science and Engineering Progress*, vol. 4, pp. 45–57, 2017.

[24] K. H. Jyothiprakash, J. Harshith, A. Sharan, K. N. Seetharamu, and Y. T. Krishnegowda, "Thermodynamic optimization of three-fluid cross-flow heat exchanger using GA and PSO heuristics," *Thermal Science and Engineering Progress*, vol. 11, pp. 289–301, 2019.

[25] A. Ranjan, R. Das, S. Pal, A. Majumder, and M. Deb, "Use of cuckoo search algorithm for performance evaluation of split elliptic shaped fins for enhanced rate of heat transfer," *Journal of Heat Transfer*, vol. 143, no. 6, article 063301, 2021.

[26] R. Das and B. Kundu, "Forward and inverse nonlinear heat transfer analysis for optimization of a constructal T-shape fin under dry and wet conditions," *International Journal of Heat and Mass Transfer*, vol. 137, pp. 461–475, 2019.

[27] R. Das and B. Kundu, "Direct and inverse approaches for analysis and optimization of fins under sensible and latent heat load," *International Journal of Heat and Mass Transfer*, vol. 124, pp. 331–343, 2018.

[28] S. B. Chin, J. J. Foo, Y. L. Lai, and K. T. Yong, "Forced convective heat transfer enhancement with perforated pin fins," *Heat and Mass Transfer*, vol. 49, no. 10, pp. 1447–1458, 2013.

[29] B. E. Launder and D. B. Spalding, *Mathematical Models of Turbulence*, Academic Press, 1973.

[30] H. L. Versteeg and W. Malalasekera, *Computational Fluid Dynamics*, Longman Group, 1995.

[31] D. Sahel, L. Bellahcene, A. Yousfi, and A. Subasi, "Numerical investigation and optimization of a heat sink having hemispherical pin fins," *International Communications in Heat and Mass Transfer*, vol. 122, article 105133, 2021.

[32] T. Hempijid and C. Kittichaikarn, "Effect of heat sink inlet and outlet flow direction on heat transfer performance," *Applied Thermal Engineering*, vol. 164, article 114375, 2020.

[33] A. Tikadar, T. C. Paul, S. K. Oudah, N. M. Abdulrazzaq, A. S. Salman, and J. A. Khan, "Enhancing thermal-hydraulic performance of counter flow mini-channel heat sinks utilizing secondary flow: numerical study with experimental validation," *International Communications in Heat and Mass Transfer*, vol. 111, article 104447, 2020.

[34] M. A. Alfellag, H. E. Ahmed, and A. S. Kherbeet, "Numerical simulation of hydrothermal performance of minichannel heat sink using inclined slotted plate-fins and triangular pins," *Applied Thermal Engineering*, vol. 164, article 114509, 2020.

[35] A. Kumar, K. Singh, and R. Das, "Response surface based experimental analysis and thermal resistance model of a thermoelectric power generation system," *Applied Thermal Engineering*, vol. 159, article 113935, 2019.